nature portfolio

https://doi.org/10.1038/s41586-023-06934-4

Supplementary information

Non-Abelian topological order and anyons on a trapped-ion processor

In the format provided by the authors and unedited

1. Supplementary Methods: Important aspects of the physical realisation

In this section we argue why the entanglement of the state as well as the leading sources of error follow the two-dimensional kagome geometry introduced in the main text. For a full description and characterisation of the device used in the experiment, see Ref. [1]. The ions are stored in a 1D ring, but their spatial ordering is dynamically and repeatedly reconfigured during execution of a quantum circuit in order to bring arbitrary pairs together for applying laser-driven two-qubit gates. These gates are the dominant source of error in the device, and operate with an average fidelity of about 99.82%. Despite the storage of ions in a 1D ring, in the state preparation and braiding protocols they are immutably assigned to the vertices of the 2D lattice defined by the Hamiltonian in Eq. (1), and all gates are local in that 2D geometry. Moreover, the extremely long coherence times of trapped ion qubits and low cross-talk afforded by the quantum charge coupled device architecture (and systematically characterized in Ref. [1]) ensure that the dominant noise processes are local and uncorrelated errors attached to each two-qubit gate. Thus even the dominant *imperfections* in our creation of these states respect the 2D geometry defined by Eq. (1).

2. Supplementary Discussion: Proof of (5) and colour algebra

Here we prove the relationship (5) between the star and logical operators, reproduced here for convenience:

$$\prod_{s\in\text{red}\ \text{✡}} A_s = (-1)^{\frac{1-\mathcal{Z}_{GH}}{2}\frac{1-\mathcal{Z}_{BV}}{2}} \times (-1)^{\frac{1-\mathcal{Z}_{GV}}{2}\frac{1-\mathcal{Z}_{BH}}{2}} \tag{A1}$$

For ease of notation, one of the three colours is singled out but it is understood that equivalent statements hold for all permutations of colours and directions. By linearity, it suffices to show that the equation holds for all computational basis states. Since we are working in the $B_t = 1$ subspace, strings of $|1\rangle$s of a given color must form closed loops on the honeycomb superlattices of that color. These loops can either be contractible or wrap around the torus. Therefore e.g., Z_{GH} acts on computational basis states by counting the parity of strings of $|1\rangle$s on green qubits wrapping around the torus in the vertical direction. The operator $(1-\mathcal{Z}_{GH})/2\times(1-\mathcal{Z}_{BV})/2$ projects into the space of computational basis states that have an odd number of blue strings in the horizontal and green strings in the vertical direction. In this space, there must be an odd number of stars where these strings cross (and these stars must necessarily be red). On the other hand, the product of CZs within a red star is -1 if and only if the star is such a crossing star, as can be verified by considering rotations of Extended Data Figure 2. Going through the same argument for the other colours and torus directions concludes the proof.

Note that (5) implies the "color algebra" (that we note here for completeness)

$$\prod_{s\in\text{red}\ \text{✡}} A_s \mathcal{X}_{BH} = \mathcal{Z}_{GH}\mathcal{X}_{BH} \prod_{s\in\text{red}\ \text{✡}} A_s \tag{A2}$$

which follows by using $\mathcal{Z}_{BH}\mathcal{X}_{BV} = -\mathcal{X}_{BV}\mathcal{Z}_{BH}$.

3. Supplementary Discussion: Uniqueness of the $\mathcal{Z} = 1$ state and Ground State Degeneracy

Here we show the uniqueness of the ground state of (1) in a given logical sector, and show that there are exactly 22 logical sectors that contain ground states. These proofs hold for tori of arbitrary sizes, not just the 3×3-torus implemented in the experiment. All of the statements in this section hold within the $B_t = 1$-subspace.

We start by fixing a logical sector through the specification of a set of $z_{cd} = \pm1$. Denote the set of kagome stars on the lattice by S (in the experiment $|S| = 9$). Select one red (s_R), one green (s_G) and one blue star (s_B). A counting argument reveals that the subspace defined by

$$\left\{ \mathcal{Z}_{cd} = z_{cd}, B_t = 1, A_s = 1 \middle| c \in \{R, G, B\}, d\ \in \{H, V\}, \forall t, s \in S\setminus\{s_R, s_G, s_B\} \right\} \tag{A3}$$

has dimension one. There are 6 logical $z_{cd}\mathcal{Z}_{cd}$ stabilisers and $2|S|$ triangular stabilisers, $2|S|-3$ of which are independent due to $\prod_t B_t = 1$ individually for each of the colors, leading to $2|S|+3$ independent stabilisers that are diagonal in the computational basis. The independence of these diagonal stabilisers follows from the same argument as in the toric code (products of Z-plaquettes wrap around the torus an even number of times). The A_s operators are independent from the logical and triangle operators since any product that does not involve all A_s of a given color (including s_R, s_G or s_B) contains off-diagonal terms. Finally, the A_s are mutually independent. To see this, pick any state in the correct logical sector with $A_s = \pm 1$. Then, this state can be transformed into a state with any other pattern of $A_s = \pm 1$ by connecting the plaquettes which are to be toggled to s_R, s_G or s_B, (depending on their color) using strings of Z operators (similar to the cleanup step of the protocol in Fig. 3). These operations do not change the B_t and logical operators. Since we have found $3|S|$ independent stabilizers on $3|S|$ qubits (and they commute in the $B_t = +1$ space) the common +1-eigenspace is exactly one-dimensional.

The state $|z_{cd}\rangle$ in this one-dimensional space can now either be a ground state or a state with energy 2, 4 or 6 above the ground state, depending on the value of A_{s_R}, A_{s_G} and A_{s_B}. Their values now simply follow from equation (5) since in the space defined above e.g.,

$$\begin{aligned} A_{s_R} &= \prod_{s \in \text{red} \,✡} A_s \\ &= (-1)^{\frac{1-\mathcal{Z}_{GH}}{2}\frac{1-\mathcal{Z}_{BV}}{2}} \times (-1)^{\frac{1-\mathcal{Z}_{GV}}{2}\frac{1-\mathcal{Z}_{BH}}{2}} \end{aligned} \tag{A4}$$

Therefore, $\prod_{s \in \text{red} \,✡} A_s = \prod_{s \in \text{green} \,✡} A_s = \prod_{s \in \text{blue} \,✡} A_s = +1$ in the logical sectors with an even number of colour-pair crossings, which, for completeness, is the set

$$\begin{aligned} (\mathcal{Z}_{RH}, \mathcal{Z}_{GH}, \mathcal{Z}_{BH}, \mathcal{Z}_{RV}, \mathcal{Z}_{GV}, \mathcal{Z}_{BV}) \in \{&000000, \\ &000001, 000010, 000011, 000100, 000101, 000110, 000111, \\ &001000, 010000, 011000, 100000, 101000, 110000, 111000, \\ &001001, 010010, 011011, 100100, 101101, 110110, 111111\}. \end{aligned}$$

where, for readability, we have labeled such bit strings with the values of the projectors $(1+\mathcal{Z})/2$ instead of $\mathcal{Z}$ (i.e., 0 or 1 instead of ± 1).

In the absence of an analytic proof, the measurement-based protocol would also allow for an experimental detection of the ground state degeneracy. To this end, a random state is first prepared on all data qubits. In a second and third step the projections $\prod_t (1+B_t)/2$ and $\prod_s (1+A_s)/2$ are applied (in that order) via coupling to and measurement of ancillary qubits. Finally the logical $\mathcal{Z}$-operators are measured. Since, on average, random states have the same overlap with all ground state sectors, we expect each of the 22 "allowed" bitstrings to appear with probability $\sim (1-\text{noise})/22$, while the 42 bitstrings "forbidden" bitstrings appear with much lower probability $\sim$ noise/42. To produce initial random states, approximate circuits may be sufficient, for example random Clifford circuits, or even random one-qubit unitaries, which have been shown to lead to reasonable result in the context of random measurements for the determination of entanglement entropies.

4. Supplementary Methods: Fidelity Lower Bound

Here, we show how to bound the fidelity per site from the experimentally measured correlation functions. Specifically we compute a lower bound on the the fidelity of the prepared state ρ with respect to the unique state that is the +1 eigenstate of the star, triangle and logical operators A_s, B_t and $\mathcal{Z}_{cd}$ (Fig. 3). We introduce the projectors (not to be confused with the braiding operators in the Borromean interferometry experiment)

$$\begin{aligned} R &= \prod_{s \in \text{red} \,✡} \frac{1+A_s}{2} \prod_{t \in \text{green} \triangleright} \frac{1+B_t}{2} \prod_{t \in \text{blue} \triangleright} \frac{1+B_t}{2} \frac{1+\mathcal{Z}_{GH}}{2} \frac{1+\mathcal{Z}_{GV}}{2} \\ G &= \prod_{s \in \text{green} \,✡} \frac{1+A_s}{2} \prod_{t \in \text{blue} \triangleright} \frac{1+B_t}{2} \prod_{t \in \text{red} \triangleright} \frac{1+B_t}{2} \frac{1+\mathcal{Z}_{BH}}{2} \frac{1+\mathcal{Z}_{BV}}{2} \\ B &= \prod_{s \in \text{blue} \,✡} \frac{1+A_s}{2} \prod_{t \in \text{red} \triangleright} \frac{1+B_t}{2} \prod_{t \in \text{green} \triangleright} \frac{1+B_t}{2} \frac{1+\mathcal{Z}_{RH}}{2} \frac{1+\mathcal{Z}_{RV}}{2}. \end{aligned} \tag{A5}$$

Here, the products run over all stars of a given color except one (which can be chosen arbitrarily) and all triangles inscribed in the stars of that color, where across all three operators one arbitrary triangle can be excluded from each color. It follows that

$$[R, G] = [G, B] = [B, R] = 0 \tag{A6}$$

$$|\psi_0\rangle\langle\psi_0| = RGB \tag{A7}$$

We now seek to bound $\langle\psi_0|\rho|\psi_0\rangle$ by the measured expectation values $\langle R\rangle = \mathrm{Tr}\rho R$, $\langle G\rangle$ and $\langle B\rangle$. Since R, G and B are commuting projectors, there exists a common orthonormal eigenbasis $|\psi_k^{rgb}\rangle$ with $r, g, b \in \{0,1\}$ that fulfills

$$\begin{aligned} R\,|\psi_k^{rgb}\rangle &= r\,|\psi_k^{rgb}\rangle \\ G\,|\psi_k^{rgb}\rangle &= g\,|\psi_k^{rgb}\rangle \\ B\,|\psi_k^{rgb}\rangle &= b\,|\psi_k^{rgb}\rangle \end{aligned} \tag{A8}$$

and k is a degeneracy label. Expanding the prepared state in this basis

$$\rho = \sum p^{rgbk}_{r'g'b'k'}\,|\psi_k^{rgb}\rangle\,\langle\psi_{k'}^{r'g'b'}| \tag{A9}$$

defines the coefficients $p^{rgbk}_{r'g'b'k'}$. Let us also introduce shorthand notation

$$P^{rgb} := \sum_k p^{rgbk}_{rgbk} \tag{A10}$$

for the sum of the diagonal elements of ρ in a given sector in the basis chosen above. In this notation, the ground state fidelity is simply $\langle\psi_0|\rho|\psi_0\rangle = P^{111}$. We then have

$$\langle R\rangle = P^{111} + P^{110} + P^{101} + P^{100} \tag{A11a}$$
$$\langle G\rangle = P^{111} + P^{110} + P^{011} + P^{010} \tag{A11b}$$
$$\langle B\rangle = P^{111} + P^{011} + P^{101} + P^{001} \tag{A11c}$$
$$1 = P^{000} + P^{001} + P^{010} + P^{011} + P^{100} + P^{101} + P^{110} + P^{111} \tag{A11d}$$

By considering (A11a)+(A11b)+(A11c)-2(A11d), we see that P^{111} is minimized if $P^{100} = P^{010} = P^{001} = P^{000} = 0$. In this case

$$P^{111} = \langle R\rangle + \langle G\rangle + \langle B\rangle - 2 \tag{A12}$$

and this is the lower bound for the fidelity. We have measured

$$\begin{aligned} \langle R\rangle &= 0.90(1) \\ \langle G\rangle &= 0.85(1) \\ \langle B\rangle &= 0.89(1) \end{aligned} \tag{A13}$$

leading to a lower bound on the global fidelity of the prepared state

$$\langle\psi_0|\rho|\psi_0\rangle \geq 0.65(2). \tag{A14}$$

The fidelity per qubit is

$$\sqrt[27]{\langle\psi_0|\rho|\psi_0\rangle} \geq 0.984(1). \tag{A15}$$

These measurements do not take into readout errors. If one wants to assess the quality of the prepared state rather than the combined quality of state preparation and measurements, one must take into account the expectation values of R, G and B after measurement error mitigation. Based on prior characterisation of the measurement error transition matrix in the device, $p(\text{measure }0|\text{qubit is }1) = 2.37\times10^{-3}$, $p(\text{measure }1|\text{qubit is }0) = 0.82\times10^{-3}$, we have computed the corrected values by writing the raw probability distribution as a matrix product state of bond dimension n_{shots} and applying the transition matrix inverse on each site (see Extended Data Figure 3 for a detailed comparison). In principle, this correction accounts for both state preparation and measurement (SPAM) error. In practice, however, measurement errors dominate state preparation errors in the device. We find

$$\begin{aligned} \langle R\rangle_{\text{SPAM error mitigated}} &= 0.94(1) \\ \langle G\rangle_{\text{SPAM error mitigated}} &= 0.89(1) \\ \langle B\rangle_{\text{SPAM error mitigated}} &= 0.93(1) \end{aligned} \tag{A16}$$

We infer that the prepared state actually has a global fidelity of

$$\langle\psi_0|\rho|\psi_0\rangle_{\text{SPAM error mitigated}} \geq 0.75(2) \tag{A17}$$

and a fidelity per qubit

$$\sqrt[27]{\langle\psi_0|\rho|\psi_0\rangle}_{\text{SPAM error mitigated}} \geq 0.990(1). \tag{A18}$$

Using equation (A11), we can also bound the fidelity from above by noticing that

$$P^{111} \leq \min\left\{\langle R\rangle, \langle G\rangle, \langle B\rangle\right\} \tag{A19}$$

We thus find

$$\langle\psi_0|\rho|\psi_0\rangle \in [0.65(2), 0.85(2)] \tag{A20}$$

$$\sqrt[27]{\langle\psi_0|\rho|\psi_0\rangle} \in [0.984(1), 0.9940(7)] \tag{A21}$$

without SPAM error mitigation and

$$\langle\psi_0|\rho|\psi_0\rangle_{\text{SPAM error mitigated}} \in [0.75(2), 0.88(1)] \tag{A22}$$

$$\sqrt[27]{\langle\psi_0|\rho|\psi_0\rangle}_{\text{SPAM error mitigated}} \in [0.990(1), 0.9955(6)] \tag{A23}$$

with SPAM error mitigation. This is compatible with the fact that the state preparation protocol uses 3 1/3 two-qubit gates per qubit with fidelity 99.82% ($99.82\%^{3.3} \approx 99.4\%$) and the fact that gate errors typically dominate errors arising from dephasing and measurement cross-talk in the trap.

5. Supplementary Discussion: Classification of the anyons

In the main text, the Hamiltonian corresponds to a gauged $\mathbb{Z}_2^3$ Symmetry-Protected Topological state [2] and therefore is in the same family of models as the twisted quantum double $\mathcal{D}^\alpha(\mathbb{Z}_2^3)$ [3–5]. This model exhibits the same topological order as that of the quantum double of $\mathcal{D}(D_4)$ [6, 7]. We elect to present the anyon content based on the twisted quantum double. A mapping relating the two conventions can be found in Extended Data Table 2.

First, recall that in the usual toric code, anyons are generated by an Abelian charge e and an Abelian flux m where $e^2 = m^2 = 1$. Both anyons are bosons, but they have -1 mutual statistics. The bound state em is an Abelian fermion. For three copies, all anyons of the toric code are generated by e_C and m_C where $C \in \{R, G, B\}$ is a color index for each copy.

The 22 anyons of the twisted quantum double $\mathcal{D}^\alpha(\mathbb{Z}_2^3)$ can be labeled similar to that of three copies of the toric code. Instead, all fluxes are non-Abelian.

1. Eight Abelian bosons generated by e_R, e_G, e_B. Because they are Abelian, they obey the usual fusion rules i.e. $e_R \times e_G = e_{RG}$.

2. Three non-Abelian bosons m_R, m_G, m_B. They braid with the corresponding charge of the same color with a -1 phase. I.e., m_R braids non-trivially with e_R, but trivially with e_G and e_B.

3. Three non-Abelian fermions $f_R = m_R \times e_R$.

4. Three non-Abelian bosons m_{RG}, m_{GB}, m_{RB}. One can interpret these as fluxes that respond to two colors. That is m_{RG} braids with both e_R and e_G, but braids trivially with e_B.

5. Three non-Abelian fermions $f_{RG} = m_{RG} \times e_R = m_{RG} \times e_G$

6. A non-Abelian semion s_{RGB}, which is a flux that responds to three colors. That is, it braids with e_R, e_G, and e_B.

7. A non-Abelian antisemion $\bar{s}_{RGB} = s_{RBG} \times e_{RGB}$

We summarize all the remaining fusion rules (up to permutation of colors and fusion of Abelian charges) in Extended Data Table 1.For example, by permuting colors, one can infer the fusion rule $m_G \times m_G = (1+e_R)(1+e_B)$ by permuting colors, and by the fusion rule $f_R \times m_G = e_R \times (m_R \times m_G) = e_R \times (m_{RG} + f_{RG}) = f_{RG} + m_{RG}$.

Next, we describe qualitatively why braiding m_G around m_B toggles the fusion outcome of each non-Abelian flux pair to e_R. The twisted quantum double realizes a gauged Symmetry-Protected Topological (SPT) phase given by the cocycle α. Such SPT phase can be realized using a decorated domain wall construction [2, 8]. Specifically, the SPT phase can be realized by a superposition of blue domain walls decorated by 1D cluster states, which itself forms a 1D SPT state under the red and green symmetries. After gauging the symmetry, the blue domain wall is allowed to end, forming the deconfined excitation m_B. Furthermore, because the domain wall was decorated with a cluster state, its end point m_B now carries a two-dimensional projective representation inherited from the end point of the cluster state, and therefore becomes a non-Abelian excitation due to this degeneracy.

The 1D cluster state protected by the red and green symmetries has the property that the ground state under antiperiodic boundary conditions of the green symmetry is odd under the red symmetry. Such a boundary condition can be enforced by introducing a single domain wall. Therefore, by braiding m_G around m_B, a green domain wall cuts through the string operator of m_B. Inheriting the property from the cluster state, the entire m_B string is now charged under the red gauge symmetry, which implies that fusing back the m_B pair will result in a red gauge charge, e_R. By an identical argument, fusing the pair of m_G back together will also result in e_R.

We now provide more technical details on the derivation of the data corresponding to the twisted quantum double [6]. Here, we consider the twisted quantum double $\mathcal{D}^\alpha(\mathbb{Z}_2^3)$, where $\alpha \in H^3(\mathbb{Z}_2^3, U(1))$ is a 3-cocycle. Conveniently, we represent the generators of the group $A = \mathbb{Z}_2^3$ by order two elements R, G, B. Thus, any group element $a \in A$ can be represented as $a = R^{\rho_a} G^{\gamma_a} B^{\beta_a}$ for $\rho_a, \gamma_a, \beta_a \in \{0, 1\}$.

For the twisted quantum double of an Abelian group A, an anyon can be labeled by a pair (a, σ) where $a \in A$ and σ is a choice of projective irreducible representation corresponding to a 2-cocycle ω_a. Such a representation Γ_a^σ satisfies

$$\Gamma_a^\sigma(b)\Gamma_a^\sigma(c) = \omega_a(b,c)\Gamma_a^\sigma(bc), \tag{A24}$$

and the 2-cocycle ω_a is related to the input 3-cocycle α via

$$\omega_a(b,c) = \frac{\alpha(a,b,c)\alpha(b,c,a)}{\alpha(b,a,c)}. \tag{A25}$$

In particular, our 3-cocycle of interest is given by

$$\alpha(a,b,c) = (-1)^{\rho_a \gamma_b \beta_c} \tag{A26}$$

which implies that

$$\omega_a(b,c) = (-1)^{\rho_a \gamma_b \beta_c + \gamma_a \rho_b \beta_c + \beta_a \rho_b \gamma_c} \tag{A27}$$

We now discuss the possible anyons for each choice of group element $a \in A$

1. $a = 1$ ($(\rho_a, \gamma_a, \beta_a) = (0,0,0)$)). In this case, the 2-cocycle ω_a is trivial. Therefore, Γ_1^σ corresponds to (linear) irreducible representations of $\mathbb{Z}_2^3$, which correspond exactly to the choice of an element in A. We can therefore label such choices as $\sigma \in A$. These correspond to the eight Abelian charges.

2. $a = R$ ($(\rho_a, \gamma_a, \beta_a) = (1,0,0)$)). We find the 2-cocycle $\omega_R(b,c) = (-1)^{\gamma_b \beta_c}$. Eq. (A24) then implies that $\Gamma_R(G)$ and $\Gamma_R(B)$ anticommute. There are two possible choices of Γ_R, which we label by $\sigma = \pm$

$$\Gamma_R^\pm(R) = \pm I, \qquad \Gamma_R^\pm(G) = X, \qquad \Gamma_R^\pm(B) = Z, \tag{A28}$$

where X, Y, Z are Pauli matrices and I is the 2×2 identity matrix. The two choices correspond to the non-Abelian flux m_R and f_R, respectively. Similarly, by permutation of colors, we can define m_G, f_G, m_B, f_B corresponding to the representation $\Gamma_G^+, \Gamma_G^-, \Gamma_B^+, \Gamma_B^-$, respectively where

$$\Gamma_G^\pm(R) = Z, \qquad \Gamma_G^\pm(G) = \pm I, \qquad \Gamma_G^\pm(B) = X, \tag{A29}$$

$$\Gamma_B^\pm(R) = X, \qquad \Gamma_B^\pm(G) = Z, \qquad \Gamma_B^\pm(B) = \pm I. \tag{A30}$$

3. $a = RG$ ($(\rho_a, \gamma_a, \beta_a) = (1,1,0)$)). We find the 2-cocycle $c_{RG}(b,c) = (-1)^{\gamma_b \beta_c + \rho_b \beta_c}$, which means that $\{\Gamma_{RG}(R), \Gamma_{RG}(B)\} = \{\Gamma_{RG}(G), \Gamma_{rg}(B)\} = 0$. There are two inequivalent choices given by

$$\Gamma_{RG}^\pm(R) = \pm X, \qquad \Gamma_{RG}^\pm(G) = X, \qquad \Gamma_{RG}^\pm(B) = Z, \tag{A31}$$

which correspond to m_{RG} and f_{RG}, respectively. Permuting the colors gives m_{GB}, f_{GB} and m_{RB}, f_{RB}.

4. $a = RGB$ ($(\rho_a, \gamma_a, \beta_a) = (1,1,1)$)). We find the 2-cocycle $\omega_{RG}(b,c) = (-1)^{\gamma_b\beta_c + \rho_b\beta_c + \rho_b\gamma_c}$, which means that all three pairs anticommute. There are two inequivalent choices given by

$$\Gamma^{\pm}_{RGB}(R) = \pm X, \qquad \Gamma^{\pm}_{RGB}(G) = \pm Y, \qquad \Gamma^{\pm}_{RGB}(B) = \pm Z, \tag{A32}$$

which correspond to s_{RGB} and $\bar{s}_{RGB}$, respectively.

For an Abelian twisted quantum double, the S and T matrices can be computed via the formula [9]

$$S_{(a,\sigma),(b,\tau)} = \frac{1}{|A|}\chi^{\sigma}_a(b)^* \chi^{\tau}_b(a)^* \qquad T_{(a,\sigma),(b,\tau)} = \delta_{a,b}\delta_{\sigma,\tau}\frac{\chi^{\sigma}_a(a)}{\chi^{\sigma}_a(1)} \tag{A33}$$

where $\chi^{\sigma}_a = \mathrm{Tr}[\Gamma^{\sigma}_a]$ is the character of the corresponding representation. In particular, we find that

$$8S_{(a,\sigma),(b,\tau)} = \begin{cases} 1 & ; a = b = 1, \\ 2 \times (-1)^{\rho_a\rho_\tau + \gamma_a\gamma_\tau + \beta_a\beta_\tau} & ; a = 1, b \neq 1, \\ 4 \times \delta_{a,b}(-1)^{\rho_a\gamma_a\beta_a + \sigma\tau} & ; a \neq 1, b \neq 1, \end{cases} \tag{A34}$$

$$\mathrm{diag}\; T_{(a,\sigma)} = \begin{cases} 1 & ; a = 1, \\ (-1)^{\sigma} \times i^{\rho_a\gamma_a\beta_a} & a \neq 1. \end{cases} \tag{A35}$$

where we remind that $\sigma \in A$ when $a = 1$ and $\sigma = \pm 1$ for $a \neq 1$. For completeness, the full matrices are

$$\begin{array}{cccccccccccccccccccccccc} & 1 & e_R & e_G & e_B & e_{RG} & e_{GB} & e_{RB} & e_{RGB} & m_R & f_R & m_G & f_G & m_B & f_B & m_{RG} & f_{RG} & m_{GB} & f_{GB} & m_{RB} & f_{RB} & s_{RGB} & \bar{s}_{RGB} \\ \mathrm{diag}\; T = & (1 & 1 & 1 & 1 & 1 & 1 & 1 & 1 & 1 & -1 & 1 & -1 & 1 & -1 & 1 & -1 & 1 & -1 & 1 & -1 & i & -i) \end{array} \tag{A36}$$

and

$$S = \frac{1}{8}\begin{pmatrix}
1 & 1 & 1 & 1 & 1 & 1 & 1 & 1 & 2 & 2 & 2 & 2 & 2 & 2 & 2 & 2 & 2 & 2 & 2 & 2 & 2 & 2 \\
1 & 1 & 1 & 1 & 1 & 1 & 1 & 1 & -2 & -2 & 2 & 2 & 2 & 2 & -2 & -2 & 2 & 2 & -2 & -2 & -2 & -2 \\
1 & 1 & 1 & 1 & 1 & 1 & 1 & 1 & 2 & 2 & -2 & -2 & 2 & 2 & -2 & -2 & -2 & -2 & 2 & 2 & -2 & -2 \\
1 & 1 & 1 & 1 & 1 & 1 & 1 & 1 & 2 & 2 & 2 & 2 & -2 & -2 & 2 & 2 & -2 & -2 & -2 & -2 & -2 & -2 \\
1 & 1 & 1 & 1 & 1 & 1 & 1 & 1 & -2 & -2 & -2 & -2 & 2 & 2 & 2 & 2 & -2 & -2 & -2 & -2 & 2 & 2 \\
1 & 1 & 1 & 1 & 1 & 1 & 1 & 1 & 2 & 2 & -2 & -2 & -2 & -2 & -2 & -2 & 2 & 2 & -2 & -2 & 2 & 2 \\
1 & 1 & 1 & 1 & 1 & 1 & 1 & 1 & -2 & -2 & 2 & 2 & -2 & -2 & -2 & -2 & -2 & -2 & 2 & 2 & 2 & 2 \\
1 & 1 & 1 & 1 & 1 & 1 & 1 & 1 & -2 & -2 & -2 & -2 & -2 & -2 & 2 & 2 & 2 & 2 & 2 & 2 & -2 & -2 \\
2 & -2 & 2 & 2 & -2 & 2 & -2 & -2 & 4 & -4 & 0 & 0 & 0 & 0 & 0 & 0 & 0 & 0 & 0 & 0 & 0 & 0 \\
2 & -2 & 2 & 2 & -2 & 2 & -2 & -2 & -4 & 4 & 0 & 0 & 0 & 0 & 0 & 0 & 0 & 0 & 0 & 0 & 0 & 0 \\
2 & 2 & -2 & 2 & -2 & -2 & 2 & -2 & 0 & 0 & 4 & -4 & 0 & 0 & 0 & 0 & 0 & 0 & 0 & 0 & 0 & 0 \\
2 & 2 & -2 & 2 & -2 & -2 & 2 & -2 & 0 & 0 & -4 & 4 & 0 & 0 & 0 & 0 & 0 & 0 & 0 & 0 & 0 & 0 \\
2 & 2 & 2 & -2 & 2 & -2 & -2 & -2 & 0 & 0 & 0 & 0 & 4 & -4 & 0 & 0 & 0 & 0 & 0 & 0 & 0 & 0 \\
2 & 2 & 2 & -2 & 2 & -2 & -2 & -2 & 0 & 0 & 0 & 0 & -4 & 4 & 0 & 0 & 0 & 0 & 0 & 0 & 0 & 0 \\
2 & -2 & -2 & 2 & 2 & -2 & -2 & 2 & 0 & 0 & 0 & 0 & 0 & 0 & 4 & -4 & 0 & 0 & 0 & 0 & 0 & 0 \\
2 & -2 & -2 & 2 & 2 & -2 & -2 & 2 & 0 & 0 & 0 & 0 & 0 & 0 & -4 & 4 & 0 & 0 & 0 & 0 & 0 & 0 \\
2 & 2 & -2 & -2 & -2 & 2 & -2 & 2 & 0 & 0 & 0 & 0 & 0 & 0 & 0 & 0 & 4 & -4 & 0 & 0 & 0 & 0 \\
2 & 2 & -2 & -2 & -2 & 2 & -2 & 2 & 0 & 0 & 0 & 0 & 0 & 0 & 0 & 0 & -4 & 4 & 0 & 0 & 0 & 0 \\
2 & -2 & 2 & -2 & -2 & -2 & 2 & 2 & 0 & 0 & 0 & 0 & 0 & 0 & 0 & 0 & 0 & 0 & 4 & -4 & 0 & 0 \\
2 & -2 & 2 & -2 & -2 & -2 & 2 & 2 & 0 & 0 & 0 & 0 & 0 & 0 & 0 & 0 & 0 & 0 & -4 & 4 & 0 & 0 \\
2 & -2 & -2 & -2 & 2 & 2 & 2 & -2 & 0 & 0 & 0 & 0 & 0 & 0 & 0 & 0 & 0 & 0 & 0 & 0 & -4 & 4 \\
2 & -2 & -2 & -2 & 2 & 2 & 2 & -2 & 0 & 0 & 0 & 0 & 0 & 0 & 0 & 0 & 0 & 0 & 0 & 0 & 4 & -4
\end{pmatrix} \tag{A37}$$

Using the S-matrix above, the fusion rules in Table 7 can be derived using the Verlinde formula [10]

$$N^K_{IJ} = \sum_L \frac{S_{IL}S_{JL}S^*_{KL}}{S_{1L}} \tag{A38}$$

where N^K_{IJ} are fusion multiplicities for the process $I \times J = \sum_K N^K_{IJ} K$, and I, J, K, L are anyons.

Next, let us demonstrate that by creating a pair of m_G and m_B anyons, braiding them and fusing each pair back together, we are left with two e_R's as fusion outcomes. To be concrete, we will consider creating a pair of m_G at positions 1 and 2 and a pair of m_B at positions 3 and 4. We then perform a full braid of m_G at position 2 and m_B at position 3, before fusing each pair back together. Note that because each flux has quantum dimension 2, the internal state forms a qubit on which the representations Γ act on.

To create a pair of m_G fluxes, we must ensure that the state transforms under the trivial representation of $\Gamma_G^+ \otimes \Gamma_G^+$. From Eq. A29, we see that the symmetry action of red, green and blue on the two sites given by Z_1Z_2, I_1I_2, X_1X_2, respectively. Therefore, the "singlet" state under this symmetry action is stabilized Z_1Z_2 and X_1X_2 (i.e. the Bell state $\frac{1}{\sqrt{2}}(|\uparrow_1\uparrow_2\rangle + |\downarrow_1\downarrow_2\rangle)$). Similarly, a pair of m_B anyons created from the vacuum is stabilized by X_3X_4 and Z_3Z_4.

In general, the full braid of an anyon (a,σ) around (b,τ) is given by the unitary operation $\Gamma^\sigma(b)_a \times \Gamma_b^\tau(a)$. In this case, we have $(a,\sigma) = (G,+)$ and $(b,\tau) = (B,+)$. Therefore, the braiding operation on sites 2 and 3 is implemented via $\Gamma_G^+(B) \times \Gamma_B^+(G) = X_2Z_3$. Thus, we see qualitatively that we are toggling the fusion channel space of the m_G pair by X, as described in the main text. To see this explicitly, conjugating the original stabilizers, we see that the state after the braiding is stabilized by $-Z_1Z_2$, X_1X_2, Z_3Z_4, $-X_3X_4$. In particular, the state satisfies $\Gamma_G^+(R)_1\Gamma_G^+(R)_2 = Z_1Z_2 = -1$, which means it is charged under the red symmetry action. This signifies that the fusion outcome of the two m_G anyons will result in e_R. Similarly, $\Gamma_B^+(R)_3\Gamma_B^+(R)_4 = X_3X_4 = -1$, implying that the two m_B anyons also fuse into e_R.

We can also demonstrate that the Borromean ring braiding of m_R, m_G and m_B results in a phase -1. The Borromean ring braiding can be deformed topologically to the following process [11]

1. Create m_R, m_G, m_B pairs at sites 1 and 2, 3 and 4, 5 and 6, respectively.

2. Braid sites 2 and 4 followed by 2 and 6

3. Braid (in the reverse direction) sites 2 and 4 followed by 2 and 6

4. Fuse each flux pair.

Braiding sites 2 and 4 is realized by the operation $\Gamma_R^+(G)_2\Gamma_G^+(R)_4 = X_2Z_4$ while braiding sites 2 and 6 is realized by $\Gamma_R^+(B)_2\Gamma_B^+(R)_6 = Z_2X_6$. Therefore, the total braiding is realized by the operation

$$(Z_2X_6)^{-1}(X_2Z_4)^{-1}(Z_2X_6)(X_2Z_4) = -1 \tag{A39}$$

6. Supplementary Discussion: Non-square degeneracy

We provide a simple argument that all Abelian anyon theories that admit a gapped boundary (which excludes for example, chiral phases) have a perfect square ground state degeneracy on a torus. If there exists a gapped boundary, then there exists a Lagrangian subgroup K of bosons which have trivial mutual braiding statistics and braids non-trivially with all other anyons outside this group. For Abelian anyon theories, $|K|^2$ is equal to the the total number of anyons (see e.g. [12]), which is also equal to the ground state degeneracy on a torus.

7. Supplementary Methods: Qubit Reuse and Circuit Optimization Techniques

Here we describe the steps we need to realize the D_4 topological order on the H2 trapped ion device. The construction requires a total of $27 + 3 = 30$ physical qubits to create 27-qubit states. During the procedure 9 ancillas need to be measured for a layer of feed-forward. It is crucial to reuse some of those ancilla qubits to fit the protocol into the maximal qubit capacity (32) of the device. We begin by rewriting Eq. (2) as

$$|\psi_0\rangle = \prod_v H_v \langle +|_P \prod_{\langle v,p\rangle} CZ_{v,p} \prod_{\langle p,\tilde{p},\tilde{\tilde{p}}\rangle} e^{\pm \frac{i\pi}{8} Z_p Z_{\tilde{p}} Z_{\tilde{\tilde{p}}}} |+\rangle_P |+\rangle_V , \tag{A40}$$

where $|+\rangle_P = |+\rangle_P|+\rangle_P|+\rangle_P$ and $|+\rangle_V = |+\rangle_V|+\rangle_V|+\rangle_V$ denote plaquette and vertex qubits over the red, green and blue sublattices. Moreover, the product over CZs also spans over three sublattices which can be decoupled, i.e,

$$\prod_{\langle v,p\rangle} CZ_{v,p} = \prod_{\langle v,p\rangle} CZ_{v,p} \prod_{\langle v,p\rangle} CZ_{v,p} \prod_{\langle v,p\rangle} CZ_{v,p}.$$

We can rearrange Eq. (A40) as

$$|\psi_0\rangle = \prod_v H_v \langle +|_P \prod_{\langle v,p\rangle} CZ_{v,p}\, |+\rangle_V \underbrace{\langle +|_P \,\langle +|_P \prod_{\langle p,\tilde{p},\tilde{\tilde{p}}\rangle} e^{\pm \frac{i\pi}{8} Z_p Z_{\tilde{p}} Z_{\tilde{\tilde{p}}}} |+\rangle_P \left(\prod_{\langle v,p\rangle} CZ_{v,p} |+\rangle_P \,|+\rangle_V \right)\left(\prod_{\langle v,p\rangle} CZ_{v,p} |+\rangle_P \,|+\rangle_V \right)}_{\text{step 1}}. \tag{A41}$$

The construction is divided into two steps. In step 1, we act on the vertex qubits of the green and blue sublattices only, and all the plaquette qubits of all three sublattices. In total, we use $(9+9) = 18$ vertex and $(3+3+3) = 9$ plaquette qubits during step 1. At the end of step 1, we measure $(3+3) = 6$ plaquette qubits of the green and blue sublattices. During step 2, we reuse the 6 measured qubits as vertex qubits of the red sublattice and act with CZ gates before also measuring the plaquette qubits of the red sublattice.

During step 1, we choose to first implement the CZ gates between the vertices and plaquette qubit. For a given color, we have $3+3=6$ CZ gates between 3 vertex and 2 plaquette qubits (e.g., we have 3 CZs between v_1, v_2, v_3, and p_1, and 3 CZs between the same vertices and p_2). Since CZ gates for the blue and green sublattices act on qubits in the $|+\rangle$ state, the action of the later 3 CZ gates can be implemented by a single two-qubit gate. This can be seen by the state-vector identity for e.g., the blue sublattice,

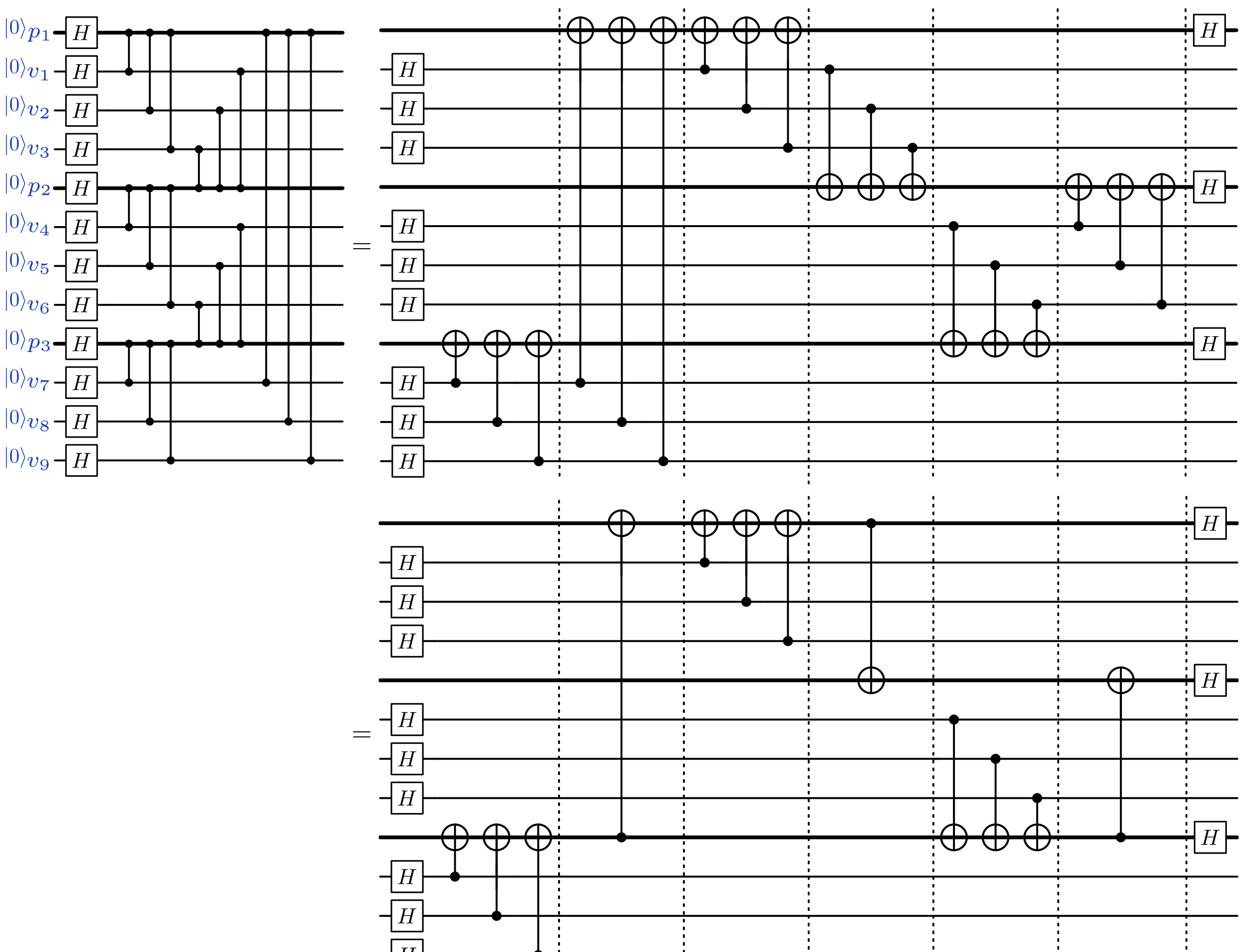

(A42)

Similar identities also holds for the green sublattice. This leads to a reduction from $3\times 6\times 2 = 36$ to $3\times 4\times 2 = 24$ two-qubit gates for the products of CZ on the blue and green sublattices.

The $\exp(\pm\frac{i\pi}{8} Z_p Z_{\tilde{p}} Z_{\tilde{\tilde{p}}})$ gate that acts on 3 plaquette qubits of distinct colors is decomposed as

$$e^{\pm \frac{i\pi}{8} Z_p Z_{\tilde{p}} Z_{\tilde{\tilde{p}}}} = \tag{A43}$$

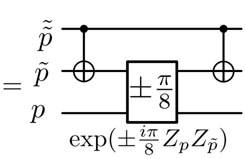

This decomposition uses the parametrised entangling gate $\text{ZZPhase}(\theta) = e^{-i\theta/2 Z\otimes Z}$ which is the native entangling gate on the device. Without any optimization, we need $18 \times 3 = 54$ gates to realize the action of $\exp(\pm\frac{i\pi}{8} Z_p Z_{\tilde{p}} Z_{\tilde{\tilde{p}}})$ gates. Since the order of qubits in (A43) does not matter, we notice that the stacked action of $\exp(+\frac{i\pi}{8} Z_0 Z_1 Z_2)$ and $\exp(-\frac{i\pi}{8} Z_1 Z_2 Z_3)$ requires not 6 but 4 two-qubit gates (Extended Data Fig. 1). By using this 'squared' implementation of the triangular $\exp(\pm\frac{i\pi}{8} Z_p Z_{\tilde{p}} Z_{\tilde{\tilde{p}}})$ gates we reduce the number of two-qubits gates for this step from 54 to $9 \times 4 = 36$.

By using these circuit optimizations, we reduce the gate count to $18 + 12 + 12 = 42$ two qubit gates for the 'CZ-chains' and 36 two-qubit gates for the $\exp(\pm\frac{i\pi}{8} Z_p Z_{\tilde{p}} Z_{\tilde{\tilde{p}}})$ gates which give us a total of $42 + 36 = 78$ two-qubit gates.

We used TKET for compiling circuits into native gates [13]. The resulting circuit (for state preparation only) consisted of 165 one-qubit gates, 60 $\text{ZZMax} = e^{-i\pi/4 Z\otimes Z}$ and 18 ZZPhase gates, while the depth of the native circuit is 56.

References

1. Moses, S. A. *et al. A Race Track Trapped-Ion Quantum Processor* May 16, 2023. arXiv: 2305.03828[quant-ph]. http://arxiv.org/abs/2305.03828 (2023).
2. Yoshida, B. Topological phases with generalized global symmetries. *Physical Review B* **93,** 155131. https://link.aps.org/doi/10.1103/PhysRevB.93.155131 (2023) (Apr. 15, 2016).
3. Dijkgraaf, R. & Witten, E. Topological gauge theories and group cohomology. *Communications in Mathematical Physics* **129,** 393–429. ISSN: 1432-0916. https://doi.org/10.1007/BF02096988 (2023) (Apr. 1, 1990).
4. Dijkgraaf, R., Pasquier, V. & Roche, P. Quasi hope algebras, group cohomology and orbifold models. *Nuclear Physics B - Proceedings Supplements* **18,** 60–72. ISSN: 0920-5632. https://www.sciencedirect.com/science/article/pii/092056329190123V (2023) (Jan. 1, 1991).
5. Hu, Y., Wan, Y. & Wu, Y.-S. Twisted quantum double model of topological phases in two dimensions. *Physical Review B* **87.** Publisher: American Physical Society, 125114. https://link.aps.org/doi/10.1103/PhysRevB.87.125114 (2023) (Mar. 11, 2013).
6. Propitius, M. d. W. *Topological interactions in broken gauge theories* Nov. 27, 1995. arXiv: hep-th/9511195. http://arxiv.org/abs/hep-th/9511195 (2023).
7. Lootens, L., Vancraeynest-De Cuiper, B., Schuch, N. & Verstraete, F. Mapping between Morita-equivalent string-net states with a constant depth quantum circuit. *Physical Review B* **105.** Publisher: American Physical Society, 085130. https://link.aps.org/doi/10.1103/PhysRevB.105.085130 (2023) (Feb. 17, 2022).
8. Chen, X., Lu, Y.-M. & Vishwanath, A. Symmetry-protected topological phases from decorated domain walls. *Nature Communications* **5.** Number: 1 Publisher: Nature Publishing Group, 3507. ISSN: 2041-1723. https://www.nature.com/articles/ncomms4507 (2023) (Mar. 26, 2014).
9. Coste, A., Gannon, T. & Ruelle, P. Finite group modular data. *Nuclear Physics B* **581,** 679–717. ISSN: 0550-3213. https://www.sciencedirect.com/science/article/pii/S0550321300002856 (2023) (Aug. 21, 2000).
10. Verlinde, E. Fusion rules and modular transformations in 2D conformal field theory. *Nuclear Physics B* **300,** 360–376. ISSN: 0550-3213. https://www.sciencedirect.com/science/article/pii/0550321388906037 (2023) (Jan. 1, 1988).
11. Wang, C. & Levin, M. Topological invariants for gauge theories and symmetry-protected topological phases. *Physical Review B* **91.** Publisher: American Physical Society, 165119. https://link.aps.org/doi/10.1103/PhysRevB.91.165119 (2023) (Apr. 15, 2015).
12. Kaidi, J., Komargodski, Z., Ohmori, K., Seifnashri, S. & Shao, S.-H. Higher central charges and topological boundaries in 2+1-dimensional TQFTs. *SciPost Physics* **13,** 067. ISSN: 2542-4653. https://scipost.org/10.21468/SciPostPhys.13.3.067 (2023) (Sept. 26, 2022).
13. Sivarajah, S. *et al.* t—ket⟩: a retargetable compiler for NISQ devices. *Quantum Science and Technology* **6.** Publisher: IOP Publishing, 014003. ISSN: 2058-9565. https://dx.doi.org/10.1088/2058-9565/ab8e92 (2023) (Nov. 2020).